Third- and fifth-harmonic generation in transparent solids with few-optical-cycle midinfrared pulses

N. Garejev,[1] I. Gražulevičiūtė,[1] D. Majus,[1] G. Tamošauskas,[1] V. Jukna,[2] A. Couairon,[2] and A. Dubietis[1,*]
[1]*Department of Quantum Electronics, Vilnius University, Saulėtekio Avenue 9, Building 3, LT-10222 Vilnius, Lithuania*
[2]*Centre de Physique Théorique, CNRS, Ecole Polytechnique, F-91128 Palaiseau, France*
(Received 27 November 2013; revised manuscript received 18 February 2014; published 24 March 2014)

We report an experimental and numerical investigation of third- and fifth-harmonic generation in a CaF_2 crystal with 20 fs (three-optical-cycle), 2 μm driving pulses. The double-peaked temporal profile of the third-harmonic pulse and its propagation dynamics was captured by means of the cross-correlation technique, showing that the third-harmonic pulse naturally consists of free and driven components propagating with different group velocities, and which occur without the splitting of the driving pulse at the fundamental frequency. Relevant characteristics of the harmonics generation process, such as the harmonics spectra, energy oscillations, and conversion efficiency, were measured as functions of propagation length and input-pulse energy and intensity. Our results demonstrate that the fifth harmonic is generated solely via cascaded four-wave mixing between the fundamental and third-harmonic frequency pulses due to cubic nonlinearity, without any detectable contribution of six-wave mixing due to quintic nonlinearity in the process.

DOI: 10.1103/PhysRevA.89.033846 PACS number(s): 42.65.Ky, 42.65.An

I. INTRODUCTION

Rapid development of high-peak-power near- and midinfrared ultrashort-pulse laser sources, which are exclusively based on optical parametric amplification [1–3], opens exciting possibilities in the emerging field of ultrafast midinfrared nonlinear optics and strong-field physics, allowing studies of nonlinear-optical phenomena in a new regime of laser-matter interaction [4]. Recent experiments established unprecedented landmarks in high-order harmonic generation in gaseous [5], solid-state [6], and liquid [7] dielectric media.

Self-focusing of ultrashort midinfrared pulses in transparent dielectrics gives rise to a qualitatively new filamentation regime [8,9], which emerges from the combined action of self-phase-modulation and anomalous group-velocity dispersion that leads to extended filament length and self-compression of the driving pulse [10,11], thus eventually producing an ultrabroadband, several-octave-spanning supercontinuum, as observed in gaseous [12–14] and solid-state media [15,16]. The ultrabroadband supercontinuum serves as a high-quality compressible seed signal for ultrafast optical parametric amplifiers [17], is used for synthesis of few-optical-cycle pulse shapes [18], and is considered as a potentially useful tool for midinfrared spectroscopy of complex molecular systems [19].

Generation of low-order odd harmonics (third, fifth, seventh, etc.) in the perturbative regime of laser-matter interaction provides a possibility of direct measurements of nonlinear-optical constants of the material, such as nonlinear-optical susceptibilities and optical nonlinearities. In the meantime, generation of low-order odd harmonics is attracting growing attention, since it might serve as an indicator enabling a test of the alleged role of the high-order Kerr effect and saturating nonlinearities in gaseous [20,21] and in solid-state media [22] in particular.

Third-harmonic generation is a frequently observed nonlinear-optical effect, which accompanies filamentation of near-infrared laser pulses in air, with [23] and without [24] the onset of supercontinuum generation; see also [25] and references therein for more details. Using midinfrared driving pulses, the wavelengths of low-order odd harmonics are shifted towards the visible and near infrared, into the transparency range of nonlinear dielectric media, where they could be readily detected by simple means. To this end, generation of third, fifth [26–28], and seventh [29] harmonics by filamentation of midinfrared laser pulses in air was recently experimentally observed. Generation of low-order odd harmonics was also reported under various experimental settings in semiconductors [30], and in liquid [31,32] and solid-state [15,16,33] dielectric media.

In this paper we report detailed experimental and numerical investigations of third- (TH) and fifth- (FH) harmonic generation in a CaF_2 sample of variable thickness as excited with 20 fs pulses at 2 μm. The cross-correlation measurements confirm the emergence of free and driven TH pulses, which produce evolving spectral interference with increasing propagation distance. A detailed study of the harmonics generation process provides direct proofs that the fifth harmonic is generated by means of only cascaded four-wave mixing between the fundamental frequency and third-harmonic pulses.

II. EXPERIMENTAL SETUP

In the experiment we used a home-built optical parametric amplifier, which was pumped by the fundamental frequency (800 nm) of the amplified Ti:sapphire laser (Spitfire-PRO, Newport-Spectra Physics) and delivered carrier-envelope phase-stable 20 fs (three-optical-cycle) pulses at a carrier wavelength of 1.98 μm with up to 10 μJ energy [34]. Its output beam was suitably attenuated and focused by an $f = +100$ mm lens onto a wedge-shaped CaF_2 sample, producing a 55-μm-diameter (FWHM) spot at the input face of the nonlinear medium. The propagation length inside the nonlinear medium was varied in the 110 μm–2 mm range by moving the CaF_2 sample across the focused beam by a motorized translation stage. The harmonics spectra were recorded using a fiber spectrometer with a 16-bit dynamic range detector (QE65000, Ocean Optics). Two automated Si

*Corresponding author: audrius.dubietis@ff.vu.lt

detectors with a sensitivity of 0.1 pJ/count and 5 fJ/count for the TH and FH energy measurements, respectively, while the energy of the fundamental frequency was measured using a standard energy meter (Ophir) with a pyroelectric sensor (PE9-SH). In that measurement, signals of the fundamental frequency, TH, and FH were separated by a fused silica prism with 60° apex angle. The cross-correlation measurements were performed by means of broadband sum-frequency generation in 0.2-mm-thick β–barium borate crystal (cut for type-I phase matching) by sampling the output pulses with 20 fs, 575 nm reference pulses from the noncollinear optical parametric amplifier (Topas-White, Light Conversion Ltd.), which was pumped by the second harmonic (400 nm) of the laser. The cross-correlation signals of either the driving pulse at fundamental frequency or the TH pulse were discriminated by setting a proper phase-matching angle of the sum-frequency-generating crystal and using a set of color glass filters.

III. THIRD-HARMONIC GENERATION

In isotropic dielectric media, TH generation is regarded as a simple nonlinear process mediated by the cubic (Kerr) nonlinearity. For efficient TH generation, the phase-matching condition $k(3\omega) = k(\omega) + k(\omega) + k(\omega)$ has to be fulfilled, where $k(\omega) = \omega n(\omega)/c$, ω is the frequency, and $n(\omega)$ is the frequency-dependent refractive index. However, owing to high dispersion in the transparency range of condensed media, TH generation is never phase matched in a collinear propagation geometry, and wave-vector mismatch, defined as $\Delta k = k(3\omega) - 3k(\omega)$, is always very large. This in turn imposes that the coherent buildup length, or simply, the coherence length, defined as $L_{\mathrm{coh}} = 2\pi/\Delta k$, is of the order of a few tens of microns and the energy conversion efficiency typically does not exceed several tenths of a percent. On the other hand, the group-velocity mismatch between the driving and TH pulses, $\nu_{13} = 1/u_1 - 1/u_3$, where u_1 and u_3 are the respective group velocities, is very large as well and becomes an equally important factor that strongly affects the dynamics of TH generation.

More specifically, in CaF_2 with 1.98 μm driving pulses the calculated $L_{\mathrm{coh}} = 78.5$ μm and $\nu_{13} = 32.4$ fs/mm. The latter converts to a walk-off length of $l_{13} = t_p/|\nu_{13}| = 620$ μm, as calculated for $t_p = 20$ fs input-pulse duration. The combination of large phase and group-velocity mismatches defines rather specific conditions for TH generation, which, in analogy with phase- and group-velocity-mismatched second-harmonic generation [35–38], leads to the occurrence of a double-peaked TH pulse, consisting of so-called free and driven components. Free and driven TH pulses are generated at the boundary between the vacuum and nonlinear medium and represent solutions of the homogenous and the inhomogenous wave equations, respectively [35]. Free and driven TH pulses propagate with different group velocities: a free TH pulse propagates with the group velocity u_3 set by the material dispersion, while a driven TH pulse propagates with the group velocity u_1 of the fundamental frequency (driving) pulse, which induces the nonlinear polarization. With propagation, the temporal separation between free and driven pulses increases as $\tau = |\nu_{13}|z$, where z is the propagation length, producing evolving interference pattern in the TH spectrum,

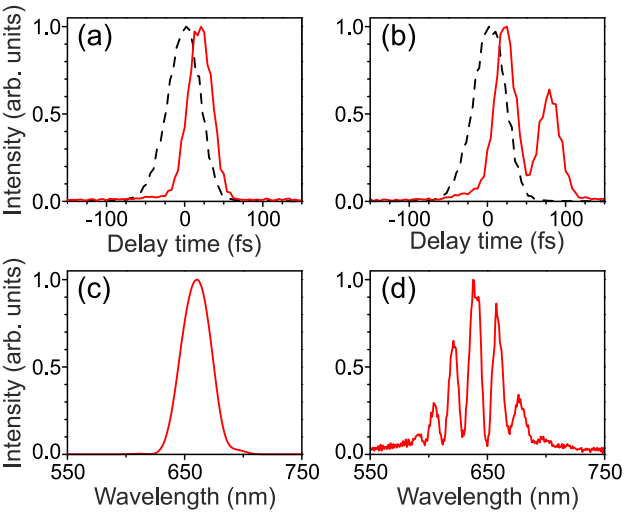

FIG. 1. (Color online) (a),(b) Cross-correlation functions of the fundamental frequency (dashed curves) and TH (solid curves) pulses, as measured with 20 fs sampling pulses, and (c),(d) TH spectra, measured at (a),(c) $z = 0.34$ mm and (b),(d) $z = 1.93$ mm of propagation in CaF_2. The input-pulse energy is 1.6 μJ. Fundamental and TH pulse intensities are not to scale.

which was recently experimentally observed in fused silica, sapphire, YAG, and CaF_2 [16].

So far, the existence of free and driven pulses in TH generation has been verified from numerical simulations and indirectly detected from spectral interference patterns [16]. In what follows, we thoroughly investigate TH generation in CaF_2 crystal of variable length and directly capture free and driven TH pulses by cross-correlation measurements. Figure 1 shows the cross-correlation functions of driving and TH pulses and the corresponding TH spectra, as recorded at $z = 0.34$ mm and $z = 1.93$ mm of propagation. At a shorter propagation distance, $z = 0.34$ mm, free and driven TH pulses still overlap and are temporally indistinguishable [Fig. 1(a)], resulting in a smooth and featureless TH spectrum, as shown in Fig. 1(c). After $z = 1.93$ mm of propagation, the free and driven pulses are separated due to the group-velocity mismatch [Fig. 1(b)]. Note that the driven TH pulse stays under the envelope of the fundamental frequency (driving) pulse, while the free TH pulse is clearly delayed; the measured temporal separation between their peaks is 59 fs, which is fairly close to the calculated value of 63 fs. A double-peaked structure of the TH pulse results in a distinct interference pattern in the TH spectrum, as seen in Fig. 1(d). A movie (see Movie 1 in the Supplemental Material [39]) shows in more detail the evolution of the TH spectrum versus propagation distance, indicating the emergence and evolution of a clear interference pattern resulting from the increase of the temporal separation between free and driven TH pulses. Note also that the driving pulse at the fundamental frequency is not considerably broadened or split in time due to the interplay between self-phase-modulation and anomalous group-velocity dispersion. It has to be mentioned that a double-peaked TH pulse was reported from air filaments under essentially different operating conditions as due to the splitting of the fundamental frequency pulse in the regime of normal group-velocity dispersion [24].

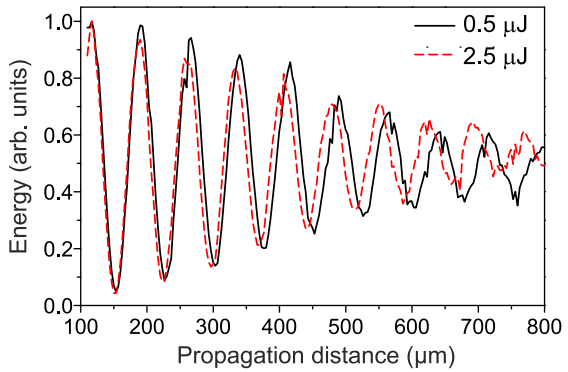

FIG. 2. (Color online) Normalized third-harmonic energy versus propagation distance, as measured with 0.5 μJ (black solid curve) and 2.5 μJ (red dashed curve) input pulses.

Figure 2 shows the variation of TH energy versus propagation distance, as measured with 0.5 and 2.5 μJ input pulses. In both cases we observe periodic oscillations of TH energy, as expected from the condition of large phase mismatch. Damping of energy oscillations results from an increase of temporal separation between the free and driven pulses due to the group-velocity mismatch [36].

At a lower input-pulse energy (0.5 μJ) the retrieved oscillation period of 76.7 ± 0.5 μm is slightly shorter than that calculated in the low-intensity limit in the plane and monochromatic wave approximation, which yields $L_{\mathrm{coh}} = 78.5$ μm. Interestingly, at a higher input-pulse energy (2.5 μJ), the oscillation period shrinks even more, down to 73.2 ± 0.8 μm; its reduction becomes obvious at longer propagation distance, as seen from Fig. 2. The detailed dependence of the oscillation period on the input-pulse energy and intensity is illustrated in Fig. 3. Here the input-pulse energy was varied in the 0.5–3.5 μJ range, so as to avoid the onset of supercontinuum generation. The tail of the supercontinuum in the visible region of the electromagnetic spectrum becomes indeed detectable for input-pulse energies above 3.5 μJ and overlaps with the TH spectrum. This has deleterious effects on the observed energy oscillations.

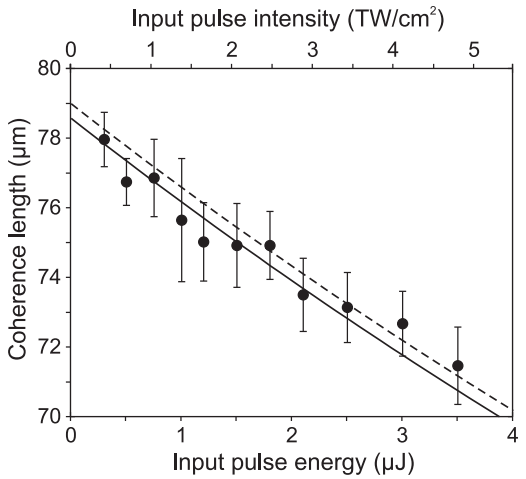

FIG. 3. Coherent buildup length as a function of the input-pulse energy and intensity. Full circles show the experimental data. Solid and dashed curves show the calculated coherent buildup length for 1.98 μm and 2.00 μm driving pulses, respectively.

The observed shortening of the coherent buildup length could be explained in simple terms, accounting for correction of the interacting wave vectors due to self- and cross-phase-modulation (intensity-dependent refractive index) effects:

$$k(\omega) = \frac{\omega}{c}[n(\omega) + n_2 I],$$
$$k(3\omega) = \frac{3\omega}{c}[n(3\omega) + 2n_2 I], \quad (1)$$

where I is the input-pulse intensity and $n_2 = 1.9 \times 10^{-16}$ cm^2/W [40] is the nonlinear refractive index of CaF_2. According to Eq. (1), an increase of the input-pulse intensity results in unequal lengthening of the interacting wave vectors, and thus in shortening of the coherence length. The calculated intensity dependence of the coherence length is in fair agreement with experimental results, as seen in Fig. 3. Also note how critically the oscillation period depends on the carrier wavelength; examples of carrier wavelengths of 1.98 μm and 2.00 μm are presented by solid and dashed lines, respectively.

IV. FIFTH-HARMONIC GENERATION

Alongside TH generation we clearly detected a fifth-harmonic signal at around 390 nm. Figure 4(a) shows TH and FH spectra, as measured with the input-pulse energy of 5 μJ at $z = 190$ μm. The respective far-field intensity profiles of FH and TH beams, as recorded with a CCD camera placed at 15 cm distance from the output face of the CaF_2 sample, are shown in Figs. 4(b) and 4(c), demonstrating that the FH and TH beams are generated on the propagation axis and have Gaussian intensity distribution, in contrast to the cone-shaped

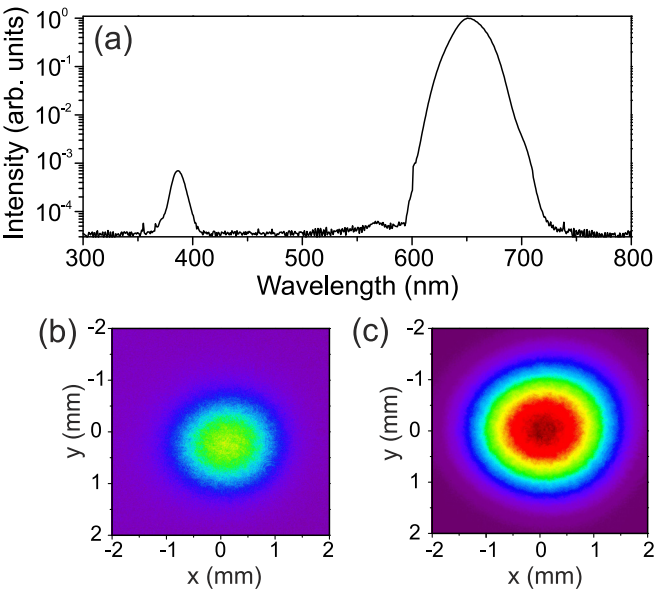

FIG. 4. (Color online) (a) TH and FH spectra as measured after $z = 190$ μm of propagation in CaF_2 with the input-pulse energy of 5 μJ. (b) and (c) show the far-field profiles of the FH and TH beams, respectively.

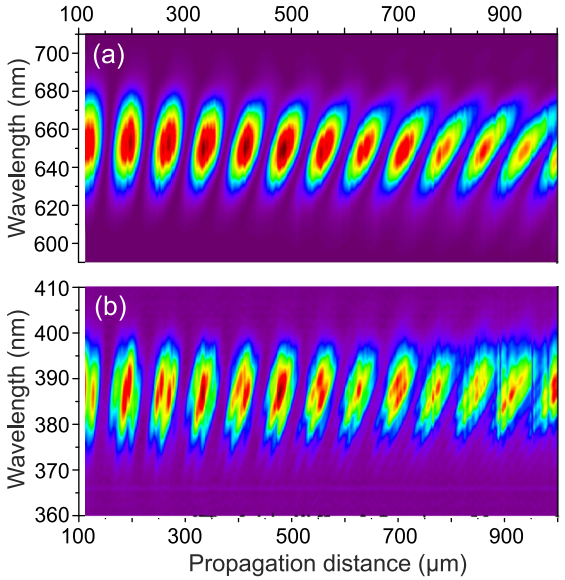

FIG. 5. (Color online) Spectra of (a) TH and (b) FH, as measured by varying the propagation length in CaF_2. The input-pulse energy is 2.8 μJ.

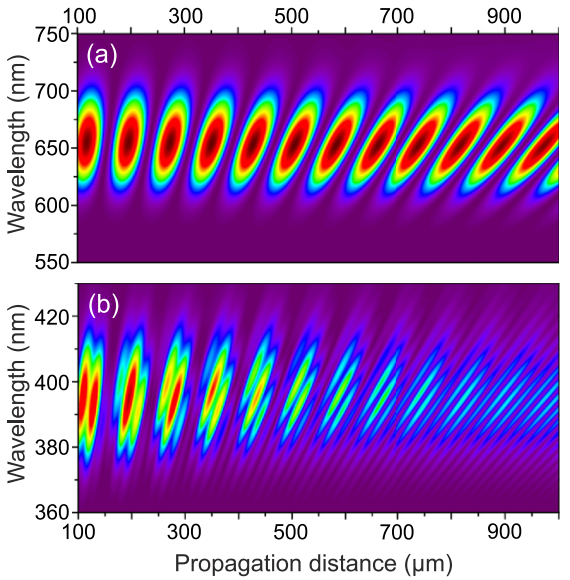

FIG. 6. (Color online) Numerically simulated (a) TH and (b) FH spectra as functions of propagation distance.

harmonic beams observed in high-numerical-aperture focusing conditions [33].

We consider three possible scenarios of FH generation. The first is based on direct FH generation (six-wave mixing) via the quintic nonlinearity $\chi^{(5)}$: $\omega+\omega+\omega+\omega+\omega=5\omega$, with phase mismatch $\Delta k = k(5\omega) - 5k(\omega)$ and estimated coherent buildup length of $L_{\rm coh} = 21.8$ μm. The two remaining scenarios are based on four-wave mixing between the fundamental frequency and its TH via the cubic nonlinearity and represent two different cascaded processes [41]. The first cascaded process could be viewed as four-wave sum-frequency generation $3\omega+\omega+\omega=5\omega$ with phase mismatch $\Delta k = k(5\omega) - k(3\omega) - 2k(\omega)$, which yields a coherent buildup length of 30.2 μm. The second cascaded process could be regarded as four-wave difference-frequency generation $3\omega + 3\omega - \omega = 5\omega$ with corresponding phase mismatch $\Delta k = k(5\omega) - 2k(3\omega) + k(\omega)$ and $L_{\rm coh} = 49.1$ μm.

In order to find out which processes are at play in the present case, we performed simultaneous spectral measurements of TH and FH radiation versus propagation distance. The experimental data are presented in Fig. 5. A sequence of TH spectral blobs, shown in Fig. 5(a), mimics the periodic oscillations of TH energy with propagation length. Wavelength integration of TH spectral blobs accurately reproduces the variation of TH energy with the oscillation period that matches perfectly the coherence length, as calculated taking into account the self- and cross-phase-modulation effects. The apparent slanting of the spectral blobs, which increases with increasing propagation distance, is attributed to interference between free and driven TH pulses: the cross section of the blobs at a fixed z yields actual shapes of TH spectra with evolving interference pattern, whose example is presented in the movie in the Supplemental Material [39]. The periodicity of FH spectral blobs, shown in Fig. 5(b), coincides with those recorded for the TH; however, with a clear onset of fine modulation, represented by much faster oscillations (sub-blobs), superimposed on the main blobs.

Figure 6 presents the results of numerical simulation, which reproduce the experimental data in great detail. The numerical model solves a simplified (one-dimensional) carrier-resolved pulse propagation equation accounting for full material dispersion and instantaneous Kerr nonlinearity. The detailed description of our model can be found elsewhere [42].

Figure 7(a) shows the measured oscillations of TH and FH spectral intensity at 650 nm and 380 nm, respectively, as extracted from Fig. 5. Figure 7(c) presents the corresponding Fourier spectra, which reveal that the FH intensity oscillates at three different frequencies, corresponding to oscillation periods of $\sim$74 μm, $\sim$28 μm, and $\sim$20 μm. The longest (74 μm) oscillation period L_1 coincides with the oscillation period of TH intensity (its coherence length), and the 28 μm period L_2 corresponds to the coherence length of FH generation via the cascaded four-wave sum-frequency generation process $\omega+\omega+3\omega=5\omega$; therefore these two periods are the signatures of the cascaded nature of FH generation. The third detected distinct oscillation period of 20 μm L_3 matches the calculated coherence length for FH generation via a pure six-wave-mixing process. On the other hand, it is easy to ascertain that the oscillation period of 20 μm results from the beating between the oscillating TH intensity and FH generation via the cascaded frequency mixing process: $L_3 = L_{\rm beat} = (1/L_1 + 1/L_2)^{-1} = 20$ μm, which in turn yields the cascaded (effective) fifth-order nonlinearity [41].

Since direct and cascaded FH generation processes provide coincident positions of the coherence peaks, unambiguous determination of their relative contributions requires more extensive analysis. Experimentally, these contributions could be verified by performing the same measurement with higher input-pulse energy and monitoring the ratio of L_2 and L_3 peak amplitudes, and expecting an increase of the L_3 peak due to the increased contribution of the direct FH generation

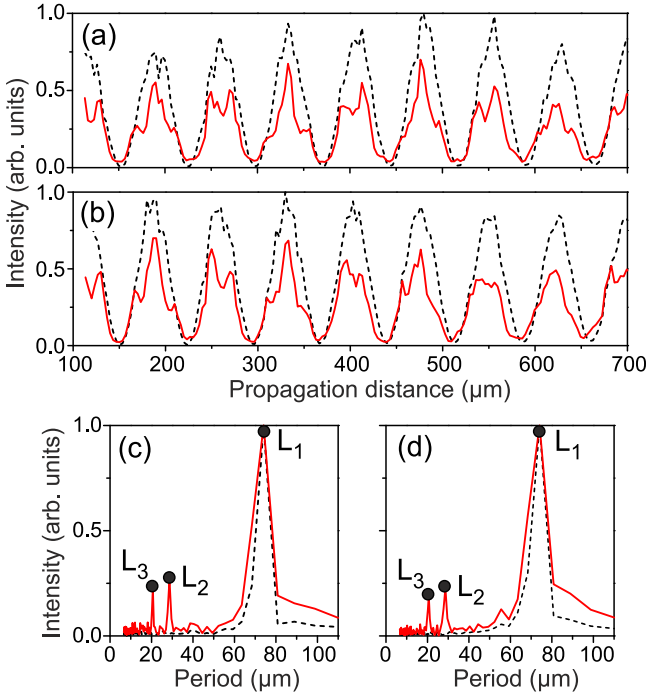

FIG. 7. (Color online) Experimentally measured oscillations of TH (black dashed curves) and FH (red solid curves) spectral intensity versus the propagation distance with the input-pulse energy of (a) 2.8 μJ and (b) 3.8 μJ. TH and FH intensities are not to scale. (c) and (d) show the corresponding Fourier spectra of TH (black dashed curves) and FH (red solid curves) oscillations. Black dots indicate the oscillation periods of the FH.

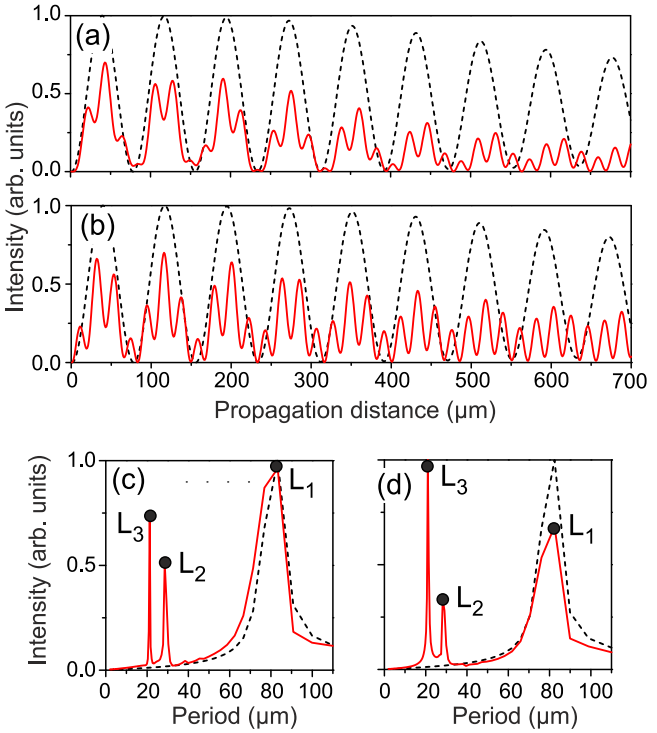

FIG. 8. (Color online) Numerically simulated oscillations of TH (black dashed curves) and FH (red solid curves) spectral intensity versus the propagation distance, using models (a) with cubic nonlinearity only, and (b) with inclusion of quintic nonlinearity. (c) and (d) show the corresponding Fourier spectra of TH (black dashed curves) and FH (red solid curves) oscillations. The input-pulse energy is 3.8 μJ.

process at higher input-pulse intensity. Figures 7(b) and 7(d) present the results obtained with higher input-pulse energy (3.8 μJ), which show that the character of the FH spectral intensity oscillations as well as the amplitudes of the L_2 and L_3 peaks in the Fourier spectra remain fairly the same. However, it must be mentioned that the input-pulse energy range in performing such a measurement is quite limited. Further increase of the input-pulse energy leads to the manifestation of unwanted nonlinear propagation effects: self-focusing of the beam leads to a marked increase of the pulse intensity with propagation, which in turn induces the change of the oscillation period, as can be easily verified from Fig. 2. Self-focusing eventually ends up with supercontinuum generation at the nonlinear focus, which continuously shifts closer to the input face of the sample as the input-pulse energy is increased. The supercontinuum radiation overlaps with the TH and FH signals and completely spoils their oscillatory character.

Therefore we extended our analysis by numerical simulations, performed using a simple model, which accounted for cubic nonlinearity only, and with an updated model, which included the quintic nonlinearity through the higher-order nonlinear refractive index n_4. In the latter simulation we used $n_4 = -2.9 \times 10^{-38}$ m^4/W^2, which was taken to be slightly higher than the value for the cascaded $n_{4,\mathrm{casc}} = -1.4 \times 10^{-38}$ m^4/W^2, as estimated from [41], thus assuming comparable contributions of the direct and cascaded nonlinearities to the FH generation processes. The results of numerical simulations using a model which accounts for cubic nonlinearity only are presented in Figs. 8(a) and 8(c), and favorably compare with the experimental data. In contrast, inclusion of the quintic nonlinearity term in the model reveals some specific features in the FH oscillation series, namely, emergence of FH peaks associated with pure six-wave mixing, which occur at the positions of TH minima, as shown in Fig. 8(b). Furthermore, the Fourier spectra of these oscillation series, as shown in Fig. 8(d), indicate a much stronger amplitude of the L_3 peak, which starts dominating the amplitudes of FH oscillations associated with cubic nonlinearity. Even a simple qualitative comparison with the experiment (see Fig. 7) shows a complete absence of these specific signatures related to direct six-wave mixing in the experimental data.

Note that neither in the experiment nor in the simulation is an oscillation with the period of 49 μm detected, which would be associated with the coherence length of the four-wave difference-frequency mixing process $3\omega + 3\omega - \omega = 5\omega$, suggesting its negligible contribution to FH generation, in line with the results of other related studies [28]. Indeed, the nonlinear polarization, oscillating at the FH frequency in this case is proportional to $\chi^{(3)} E_{\mathrm{TH}}^2 E^*$, where E denotes the complex amplitude of the electric field and is much smaller than that produced by the first cascaded process, which yields a nonlinear polarization proportional to $\chi^{(3)} E^2 E_{\mathrm{TH}}$.

Finally, we carried out measurements and numerical simulations of the harmonics energy as a function of the input-pulse energy and intensity at a fixed propagation length. The

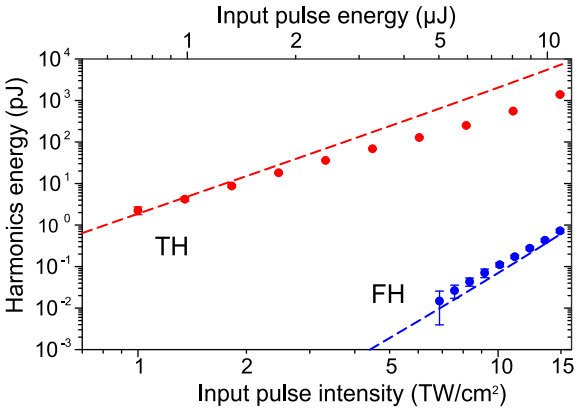

FIG. 9. (Color online) Measured (full circles) and numerically simulated (dashed lines) TH and FH energy as functions of the input-pulse energy and intensity.

measurements were performed over a wide input-pulse energy (intensity) range by setting the propagation length $z = 120\ \mu$m in the nonlinear medium, which coincides with the first experimentally accessible energy conversion maximum, and whose shift due to the intensity-dependent phase-matching condition is very small and where nonlinear propagation effects of the beam (self-focusing and filamentation) are still negligible. This in turn guaranteed that there was no supercontinuum generation up to the highest input-pulse energy used. Note that in this measurement we were able to reliably detect the FH signal in a single-shot regime only with input-pulse energy higher than 5 μJ, whereas in the spectral measurements FH spectra were detected at much lower input-pulse energy due to the possibility of increasing the acquisition time of the spectrometer. Figure 9 shows the measured and numerically simulated trends of TH and FH energy with increasing input-pulse energy (intensity). The energy curves of both harmonics exhibit a power dependence (linear on a log-log scale) and do not saturate in the investigated input-pulse intensity range.

The measured TH energy trend coincides with that obtained from the numerical simulations within the range of low input-pulse energies; however, at high input-pulse energies the measured TH energy values are consistently lower. On the other hand, there is almost perfect agreement between the experimental and numerical data on FH conversion. The disagreement between measured and numerically simulated TH energy at high input-pulse energies could be attributed to limitations of the simplified one-dimensional numerical model; however, the discrepancy obtained is not essential in terms of evaluation of ratio between FH and TH yields, which might serve as an indicator of the role of higher-order Kerr nonlinearities [20]. More precisely, at the highest input-pulse energy of 10.85 μJ, which is equivalent to an input-pulse intensity of 14.9 TW/cm^2, the measured TH and FH energies were 1.4 nJ and 0.72 pJ, respectively. The corresponding measured TH and FH conversion efficiencies were 1.3×10^{-4} and 6.6×10^{-8}. The experimental values are consistent with data from numerical simulations, which yield TH and FH energies of 7.5 nJ and 0.64 pJ, respectively, and which convert to corresponding energy conversions of 6.8×10^{-4} and 5.8×10^{-8}. The experimental and numerically simulated ratios between FH and TH yields are found as 5.1×10^{-4} and 8.5×10^{-5}, respectively. These results are very much in line with analogous experimental values obtained from filamentation in air [27] and agree with numerical estimations of these parameters using a standard model of intense pulse propagation in a dielectric medium with instantaneous nonlinearity and linear dependence of the refractive index on the intensity [20].

V. CONCLUSIONS

In this work we carried out a detailed experimental and numerical investigation of third- and fifth-harmonic generation in CaF_2 crystals of variable thickness with 20 fs pulses at 2 μm. The cross-correlation measurements directly retrieved a double-peaked temporal structure of TH radiation, consisting of free and driven components, which are generated at the boundary of a vacuum and a nonlinear dielectric medium in the conditions of large phase and group-velocity mismatch. The free and driven TH pulses propagate with different group velocities; the temporal separation between the pulses increases with propagation and produces an evolving interference pattern in the TH spectrum. We also demonstrated that the period of the TH energy oscillations (the coherent buildup length) slightly shrinks with an increase of the input-pulse energy (intensity), and the observed change was explained by wave-vector lengthening of the interacting waves due to self- and cross-phase-modulation effects.

A detailed measurements of TH and FH spectra as functions of propagation distance, followed by analysis of TH and FH oscillation periods, and combined with supporting numerical simulations, showed that the FH is generated via cascaded four-wave mixing between the fundamental and third harmonics, $5\omega = 3\omega + \omega + \omega$. A good agreement between the experiments and numerical simulations was obtained when the model accounted for cubic nonlinearity only, whereas the agreement is lost when quintic nonlinearity is included, suggesting that the contribution of pure six-wave mixing due to quintic nonlinearity in the FH generation process is undetectable with input-pulse intensities up to 5 TW/cm^2, which are typical input-pulse intensity values used in filamentation, supercontinuum generation, and self-compression experiments in bulk solid-state media in the midinfrared spectral range [8–11,15,16]. The measured power law of the TH and FH energy dependence on the input-pulse energy along with the related low conversion efficiencies allow the extension of our conclusion regarding the negligible role of higher-order nonlinearities for input-pulse intensities up to 15 TW/cm^2.

ACKNOWLEDGMENTS

This research was funded by the European Social Fund under the Global Grant measure, Grant No. VP1-3.1-ŠMM-07-K-03-001. The authors acknowledge G. Valiulis for useful discussions.

[1] D. Brida, C. Manzoni, G. Cirmi, M. Marangoni, S. Bonora, P. Villoresi, S. De Silvestri, and G. Cerullo, J. Opt. **12**, 013001 (2010).

[2] G. Andriukaitis, T. Balčiūnas, S. Ališauskas, A. Pugžlys, A. Baltuška, T. Popmintchev, M.-C. Chen, M. M. Murnane, and H. C. Kapteyn, Opt. Lett. **36**, 2755 (2011).

[3] J. Biegert, P. K. Bates, and O. Chalus, IEEE J. Sel. Top. Quantum Electron. **18**, 531 (2012).

[4] C. Vozzi, M. Negro, and S. Stagira, J. Mod. Opt. **59**, 1283 (2012).

[5] T. Popmintchev, M.-C. Chen, D. Popmintchev, P. Arpin, S. Brown, S. Ališauskas, G. Andriukaitis, T. Balčiunas, O. D. Mücke, A. Pugžlys, A. Baltuška, B. Shim, S. E. Schrauth, A. Gaeta, C. Hernández-Garcia, L. Plaja, A. Becker, A. Jaron-Becker, M. M. Murnane, and H. C. Kapteyn, Science **336**, 1287 (2012).

[6] S. Ghimire, A. D. DiChiara, E. Sistrunk, P. Agostini, L. F. DiMauro, and D. A. Reis, Nat. Phys. **7**, 138 (2011).

[7] A. D. DiChiara, E. Sistrunk, T. A. Miller, P. Agostini, and L. F. DiMauro, Opt. Express **17**, 20959 (2009).

[8] M. Durand, A. Jarnac, A. Houard, Y. Liu, S. Grabielle, N. Forget, A. Durécu, A. Couairon, and A. Mysyrowicz, Phys. Rev. Lett. **110**, 115003 (2013).

[9] M. Durand, K. Lim, V. Jukna, E. McKee, M. Baudelet, A. Houard, M. Richardson, A. Mysyrowicz, and A. Couairon, Phys. Rev. A **87**, 043820 (2013).

[10] E. O. Smetanina, V. O. Kompanets, A. E. Dormidonov, S. V. Chekalin, and V. P. Kandidov, Laser Phys. Lett. **10**, 105401 (2013).

[11] M. Hemmer, M. Baudisch, A. Thai, A. Couairon, and J. Biegert, Opt. Express **21**, 28095 (2013).

[12] D. Kartashov, S. Ališauskas, A. Pugžlys, A. Voronin, A. Zheltikov, M. Petrarca, P. Béjot, J. Kasparian, J.-P. Wolf, and A. Baltuška, Opt. Lett. **37**, 3456 (2012).

[13] M. Cheng, A. Reynolds, H. Widgren, and M. Khalil, Opt. Lett. **37**, 1787 (2012).

[14] D. Kartashov, S. Ališauskas, A. Pugžlys, A. Voronin, A. Zheltikov, M. Petrarca, P. Béjot, J. Kasparian, J.-P. Wolf, and A. Baltuška, Opt. Lett. **38**, 3194 (2013).

[15] F. Silva, D. R. Austin, A. Thai, M. Baudisch, M. Hemmer, D. Faccio, A. Couairon, and J. Biegert, Nat. Commun. **3**, 807 (2012).

[16] J. Darginavičius, D. Majus, V. Jukna, N. Garejev, G. Valiulis, A. Couairon, and A. Dubietis, Opt. Express **21**, 25210 (2013).

[17] I. Nikolov, A. Gaydardzhiev, I. Buchvarov, P. Tzankov, F. Noack, and V. Petrov, Opt. Lett. **32**, 3342 (2007).

[18] F. Hagemann, O. Gause, L. Wöste, and T. Siebert, Opt. Express **21**, 5536 (2013).

[19] C. Calabrese, A. M. Stingel, L. Shen, and P. B. Petersen, Opt. Lett. **37**, 2265 (2012).

[20] M. Kolesik, E. M. Wright, and J. V. Moloney, Opt. Lett. **35**, 2550 (2010).

[21] M. Kolesik, D. Mirell, J.-C. Diels, and J. V. Moloney, Opt. Lett. **35**, 3685 (2010).

[22] B. Borchers, C. Brée, S. Birkholz, A. Demircan, and G. Steinmeyer, Opt. Lett. **37**, 1541 (2012).

[23] M. Kolesik, E. M. Wright, A. Becker, and J. V. Moloney, Appl. Phys. B: Lasers Opt. **85**, 531 (2006).

[24] N. Akozbek, A. Iwasaki, A. Becker, M. Scalora, S. L. Chin, and C. M. Bowden, Phys. Rev. Lett. **89**, 143901 (2002).

[25] Y. Liu, M. Durand, A. Houard, B. Forestier, A. Couairon, and A. Mysyrowicz, Opt. Commun. **284**, 4706 (2011).

[26] J. Ni, J. Yao, B. Zeng, W. Chu, G. Li, H. Zhang, C. Jing, S. L. Chin, Y. Cheng, and Z. Xu, Phys. Rev. A **84**, 063846 (2011).

[27] G. O. Ariunbold, P. Polynkin, and J. V. Moloney, Opt. Express **20**, 1662 (2012).

[28] D. Kartashov, S. Ališauskas, A. Pugžlys, A. A. Voronin, A. M. Zheltikov, and A. Baltuška, Opt. Lett. **37**, 2268 (2012).

[29] A. Nath, J. A. Dharmadhikari, A. K. Dharmadhikari, and D. Mathur, Opt. Lett. **38**, 2560 (2013).

[30] A. H. Chin, O. G. Calderón, and J. Kono, Phys. Rev. Lett. **86**, 3292 (2001).

[31] R. Zurl and H. Graener, Appl. Phys. B **66**, 213 (1998).

[32] G. Mao, Y. Wu, and K. D. Singer, Opt. Express **15**, 4857 (2007).

[33] K. D. Moll, D. Homoelle, A. L. Gaeta, and R. W. Boyd, Phys. Rev. Lett. **88**, 153901 (2002).

[34] J. Darginavičius, N. Garejev, and A. Dubietis, Opt. Lett. **37**, 4805 (2012).

[35] M. Mlejnek, E. M. Wright, J. V. Moloney, and N. Bloembergen, Phys. Rev. Lett. **83**, 2934 (1999).

[36] V. Roppo, M. Centini, C. Sibilia, M. Bertolotti, D. de Ceglia, M. Scalora, N. Akozbek, M. J. Bloemer, J. W. Haus, O. G. Kosareva, and V. P. Kandidov, Phys. Rev. A **76**, 033829 (2007).

[37] E. Fazio, F. Pettazzi, M. Centini, M. Chauvet, A. Belardini, M. Alonzo, C. Sibilia, M. Bertolotti, and M. Scalora, Opt. Express **17**, 3141 (2009).

[38] G. Valiulis, V. Jukna, O. Jedrkiewicz, M. Clerici, E. Rubino, and P. Di Trapani, Phys. Rev. A **83**, 043834 (2011).

[39] See Supplemental Material at http://link.aps.org/supplemental/10.1103/PhysRevA.89.033846 for the evolution of the interference pattern in the TH spectrum as measured by gradually increasing propagation distance in CaF_2 crystal.

[40] D. Milam, M. J. Weber, and A. J. Glass, Appl. Phys. Lett. **31**, 822 (1977).

[41] M. Bache, F. Eilenberger, and S. Minardi, Opt. Lett. **37**, 4612 (2012).

[42] A. Couairon, E. Brambilla, T. Corti, D. Majus, O. de J. Ramírez-Góngora, and M. Kolesik, Eur. Phys. J. Special Topics **199**, 5 (2011).